LBL-34112
UC-405
Preprint

Lawrence Berkeley Laboratory

UNIVERSITY OF CALIFORNIA

Physics Division

Mathematics Department

To be Submitted for Publication

A High Order Vortex Method for Patches of Constant Vorticity

H.Y. Wang

May 1993

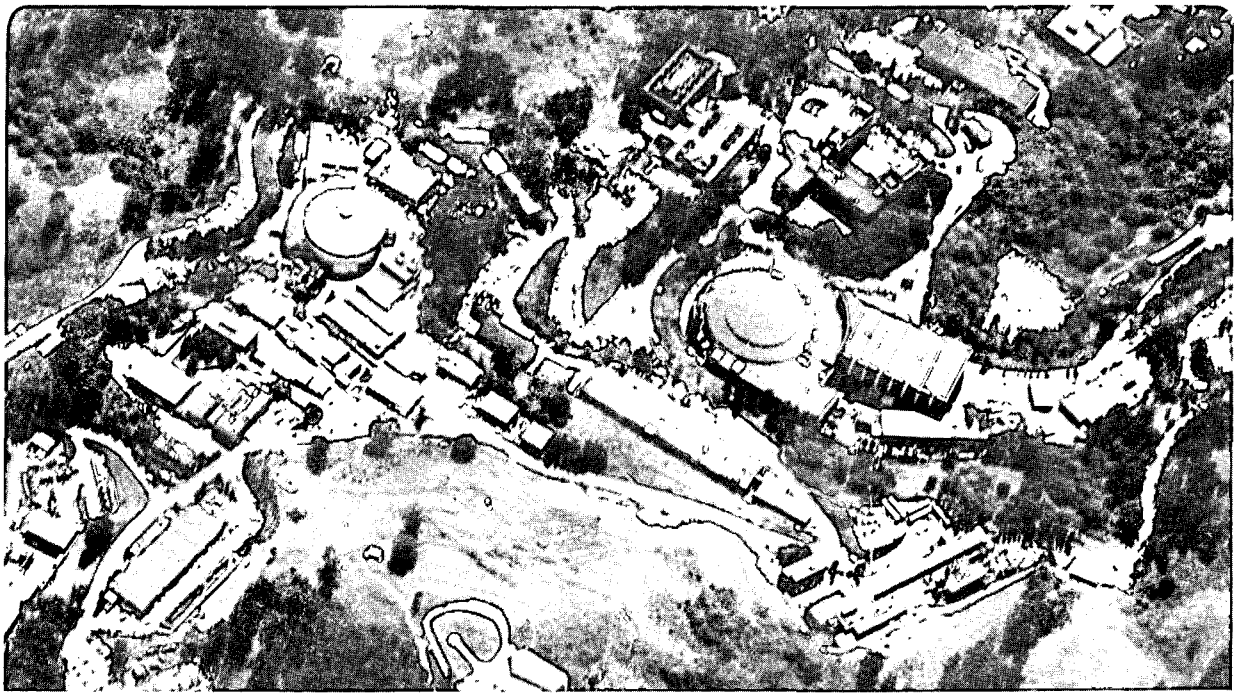

LOAN COPY
Circulates
for 4 weeks
Bldg. 50 Library.
Copy 2
LBL-34112

Prepared for the U.S. Department of Energy under Contract Number DE-AC03-76SF00098

DISCLAIMER

This document was prepared as an account of work sponsored by the United States Government. While this document is believed to contain correct information, neither the United States Government nor any agency thereof, nor the Regents of the University of California, nor any of their employees, makes any warranty, express or implied, or assumes any legal responsibility for the accuracy, completeness, or usefulness of any information, apparatus, product, or process disclosed, or represents that its use would not infringe privately owned rights. Reference herein to any specific commercial product, process, or service by its trade name, trademark, manufacturer, or otherwise, does not necessarily constitute or imply its endorsement, recommendation, or favoring by the United States Government or any agency thereof, or the Regents of the University of California. The views and opinions of authors expressed herein do not necessarily state or reflect those of the United States Government or any agency thereof or the Regents of the University of California.

LBL - 34112
UC-405

A High Order Vortex Method for Patches of Constant Vorticity [1]

Hong Yun Wang

Department of Mathematics and Lawrence Berkeley Laboratory

University of California, Berkeley, CA 94720

May 13, 1993

[1]This work was supported in part by the Applied Mathematical Sciences subprogram of the Office of Energy Research, U.S. Department of Energy, under contract DE-AC03-76SF-00098, and in part by the National Science Foundation under grant number DMS89-19074.

AMS(MOS) Subject classifications: 65P99, 65P15, 77A99

Key words: vortex method, vortex patch, singularity, numerical cancellation

Running title: a high order vortex method

Mailing address:

Hong Yun Wang

Department of Mathematics

University of California

Berkeley, CA 94720

Abstract

A high order vortex method is described for solving the two dimensional incompressible Euler equation in the case where the flow field can be represented by patches of constant vorticity. It is a continuation of Buttke's adaptive vortex method [J. Comput. Phys. 89, 161 (1990)]. In our method, each patch is approximated by a polygon plus a residual part. Through the introduction of an explicit formula for the velocity induced by a triangle, and the approximation of the residual part by vortex sheets, the fluid velocity is obtained with third order accuracy. Numerical cancellation is carefully avoided. Two numerical simulations are carried out. In the problem of two circular patches initially separated by a distance of half their radius, we study the curvature of boundary near the point which was previously observed as a cusp. Our numerical experiments show that the curvature there is finite.

Introduction

Introduced here is a method for investigating the two dimensional evolution of a piecewise constant vorticity distribution in an inviscid, incompressible and unbounded fluid.

When finite difference methods are used to simulate these flows, a high mesh resolution is required to avoid introducing grid scale dissipation and dispersion errors. To overcome these difficulties, Chorin [1] proposed vortex methods which advect vortex blobs according to the fluid velocity calculated from the existing vorticity distribution. The methods were designed to simulate the dynamics of arbitrary vorticity distributions in two or three dimensions. For the particular problem of patches of constant vorticity, it is uneconomical to apply this general method directly, therefore a special method should be sought.

Zabusky, Hughes and Roberts [2] presented a contour dynamics method in which fluid velocity is determined by integrating an appropriate kernel function along the boundaries of the patches. Contour dynamics can yield high resolution results with only a moderate amount of computation if the boundaries of patches are relatively simple. However, for contours which become stretched, numerical cancellation may cause a loss of accuracy.

Buttke [3] presented an adaptive vortex method for patches of constant vorticity in two dimensions. In his method, cells of multiple scales are used to represent the patches so that the number of cells needed to approximate a patch is proportional to the length of the boundary of the patch, and inversely proportional to the width of the smallest cell used. This method does eliminate the numerical cancellation and works well even if the patches become stretched and deformed severely. There are three sources of error in this method. The total error takes the following form:

$$Error \approx C_1 \Delta\xi + C_2(\Delta s)^2 + C_3(\Delta t)^4$$

where Δt is the time step, Δs is the maximum distance between adjacent nodes and $\Delta\xi$ is the width of the smallest square cell employed in the method. Usually, the dominant part of the error is $C_1\Delta\xi$ which comes from approximating a polygon by square cells.

Based on Buttke's idea, we now develop a high order vortex method for patches of constant vorticity. In order to get high order accuracy in space, we describe a patch more accurately than taking it as a polygon. In our method, the numerical nodes along the boundary of a patch are linked sequentially to form a polygon. The polygon is then cut into triangles. The difference between the patch and the polygon is called the residual part.

It consists of many lens-shaped areas. We calculate the velocity at a point $Q = (x_0, y_0)$ by integrating the kernel function (which is the velocity induced by a unit point vortex at (x, y))

$$(u, v) = \frac{1}{2\pi}\left[\frac{(y - y_0)}{(x - x_0)^2 + (y - y_0)^2} \ , \ \frac{-(x - x_0)}{(x - x_0)^2 + (y - y_0)^2}\right]$$

on the polygon and the residual part. We derive explicit formulas for the velocity induced by a triangle and discuss the way to avoid numerical cancellation. While the integral of the kernel on the polygon is calculated exactly by summing the contributions of all triangles, the residual part itself cannot be fully determined by a finite number of nodes, so its contribution has to be obtained approximately. Fortunately, the contribution of the residual part is so small $(\sim O(\triangle s)^2)$ that to obtain a third order method, we only need its first order approximation. We approximate each lens-shaped vortex area in the residual part by a vortex sheet. The integral on the residual part is evaluated by summing the contributions of these vortex sheets.

In the first section, we derive the formula for the velocity induced by a triangle. In the second section, we point out the numerical singularities in the formula and discuss how to avoid them. In the third section, we describe a method for calculating the fluid velocity and a principle for adding and removing numerical points during calculation. In the fourth section, we

discuss the error of the method. In the fifth section, we give two numerical examples. In the second numerical example, we study the curvature of boundary in the region where the possibility of forming a singularity in finite time was discussed in [4, 5, 6, 7]. Our observation is that the curvature of boundary in that region converges numerically to a finite value as we refine the time step and the space step.

1 The velocity induced by a triangle

Euler's equation in two dimensions is [8]

$$\frac{\partial \vec{u}}{\partial t} + (\vec{u} \cdot \nabla)\vec{u} = -\frac{\nabla p}{\rho} \tag{1}$$

where $\vec{u} = (u, v)$ is the velocity of the fluid, t is the time, p is the pressure and ρ is the density of the fluid.

In the incompressible case where $\nabla \cdot \vec{u} = \frac{\partial u}{\partial x} + \frac{\partial v}{\partial y} = 0$, (1) becomes

$$\frac{\partial \omega}{\partial t} + (\vec{u} \cdot \nabla)\omega = 0 \tag{2}$$

where $\omega = \frac{\partial v}{\partial x} - \frac{\partial u}{\partial y}$ is the vorticity of the fluid.

(2) indicates that the vorticity is advected with the fluid. For the problem of vortex patches, it implies that during the evolution, a patch will always retain same constant vorticity even though it may deform severely.

To solve the problem of vortex patches, we only need to follow the boundaries of these patches.

The incompressibility allows us to define the flux function ψ as

$$u = \psi_y \quad , \quad v = -\psi_x \quad . \tag{3}$$

Combining the definition of vorticity and (3), we find

$$\psi_{xx} + \psi_{yy} = -\omega \quad . \tag{4}$$

From (3) and (4), we can express the fluid velocity $\vec{u} = (u, v)$ as

$$u(x_0, y_0, t) = \frac{1}{2\pi} \int_{R^2} \frac{(y - y_0)\omega(x, y, t)}{(x - x_0)^2 + (y - y_0)^2} dxdy \tag{5}$$

$$v(x_0, y_0, t) = \frac{1}{2\pi} \int_{R^2} \frac{-(x - x_0)\omega(x, y, t)}{(x - x_0)^2 + (y - y_0)^2} dxdy \tag{6}$$

Since $\omega(x, y, t)$ is a piece-wise constant function, (5) and (6) become

$$u(x_0, y_0, t) = \frac{1}{2\pi} \sum_{i=1}^{k} \omega_i \int_{\Omega_i(t)} \frac{(y - y_0)}{(x - x_0)^2 + (y - y_0)^2} dxdy \tag{7}$$

$$v(x_0, y_0, t) = \frac{1}{2\pi} \sum_{i=1}^{k} \omega_i \int_{\Omega_i(t)} \frac{-(x - x_0)}{(x - x_0)^2 + (y - y_0)^2} dxdy \tag{8}$$

where k is the number of patches, $\Omega_i(t)$ is the region of the ith patch and ω_i is the vorticity of the ith patch. As noted above, ω_i will remain unchanged during the evolution.

A patch can be approximated by a polygon which can be cut into triangles. Therefore we take the triangle as the basic element for approximating

a patch. In order to calculate the integrals on $\Omega_i(t)$ in (7) and (8), we now derive the formula for the velocity induced by a triangle.

We translate and rotate the coordinate system, so that the triangle is in the position as in Fig.1. Three vertices of the triangle are $Q_1 = (-c, 0)$, $Q_2 = (c, 0)$ and $Q_3 = (a, b)$. At the beginning, we assume that the point $Q = (x_0, y_0)$ is outside the triangle. The induced velocity is given by

$$u(x_0, y_0) = \frac{\omega}{2\pi} \int_\triangle \frac{(y - y_0)}{(x - x_0)^2 + (y - y_0)^2} dxdy \stackrel{def}{=} \frac{\omega}{2\pi} I(x_0, y_0) \tag{9}$$

$$v(x_0, y_0) = \frac{\omega}{2\pi} \int_\triangle \frac{-(x - x_0)}{(x - x_0)^2 + (y - y_0)^2} dxdy \stackrel{def}{=} \frac{\omega}{2\pi} J(x_0, y_0) \tag{10}$$

We now calculate J and I

$$\begin{aligned} J &= \int_0^b dy \int_{-c+(a+c)y/b}^{c+(a-c)y/b} \frac{-(x - x_0)}{(x - x_0)^2 + (y - y_0)^2} dx \\ &= \int_0^b dy \left\{ -\frac{1}{2} \log \left[(x - x_0)^2 + (y - y_0)^2 \right] \Bigg|_{x=-c+(a+c)y/b}^{x=c+(a-c)y/b} \right\} \end{aligned} \tag{11}$$

Integration by parts gives

$$\begin{aligned} J &= \int_0^b \frac{1}{2} y d \left\{ \log \left[(x - x_0)^2 + (y - y_0)^2 \right] \Bigg|_{x=-c+(a+c)y/b}^{x=c+(a-c)y/b} \right\} \\ &= \int_0^b y \left\{ \frac{(y - \beta_1)}{(y - \beta_1)^2 + \gamma_1^2} - \frac{(y - \beta_2)}{(y - \beta_2)^2 + \gamma_2^2} \right\} dy \\ &= \frac{\beta_1}{2} \log \frac{[(b - \beta_1)^2 + \gamma_1^2]}{\beta_1^2 + \gamma_1^2} - \frac{\beta_2}{2} \log \frac{[(b - \beta_2)^2 + \gamma_2^2]}{\beta_2^2 + \gamma_2^2} \\ &\quad -|\gamma_1| \left(\frac{\pi}{2} - \arctan \frac{\gamma_1^2 + \beta_1^2 - b\beta_1}{b|\gamma_1|} \right) \\ &\quad +|\gamma_2| \left(\frac{\pi}{2} - \arctan \frac{\gamma_2^2 + \beta_2^2 - b\beta_2}{b|\gamma_2|} \right) \end{aligned} \tag{12}$$

where

$$\beta_1 = \frac{y_0 + \frac{a-c}{b}(x_0 - c)}{1 + \frac{(a-c)^2}{b^2}} \quad , \quad \gamma_1 = \frac{(a-c)\frac{y_0}{b} - (x_0 - c)}{1 + \frac{(a-c)^2}{b^2}} \tag{13}$$

$$\beta_2 = \frac{y_0 + \frac{a+c}{b}(x_0 + c)}{1 + \frac{(a+c)^2}{b^2}} \quad , \quad \gamma_2 = \frac{(a+c)\frac{y_0}{b} - (x_0 + c)}{1 + \frac{(a+c)^2}{b^2}} \, . \tag{14}$$

Similarly for I, we have

$$\begin{aligned} I = \frac{\gamma_1}{2}\log\frac{[(b-\beta_1)^2+\gamma_1^2]}{\beta_1^2+\gamma_1^2} - \frac{\gamma_2}{2}\log\frac{[(b-\beta_2)^2+\gamma_2^2]}{\beta_2^2+\gamma_2^2} \\ +\beta_1 \mathrm{sign}(\gamma_1)\left(\frac{\pi}{2} - \arctan\frac{\gamma_1^2+\beta_1^2-b\beta_1}{b|\gamma_1|}\right) \\ -\beta_2 \mathrm{sign}(\gamma_2)\left(\frac{\pi}{2} - \arctan\frac{\gamma_2^2+\beta_2^2-b\beta_2}{b|\gamma_2|}\right) \end{aligned} \tag{15}$$

(12) and (15) are valid only for a point (x_0, y_0) which is outside the triangle and satisfies $\gamma_1 \neq 0$ and $\gamma_2 \neq 0$.

What happens to a point (x_0, y_0) inside the triangle? When a numerical node is inside the triangle, it certainly is inside the polygon containing the triangle. Approximately, we assume it is inside the vortex patch. This means that either two patches overlap, or two parts of a patch overlap. Neither of these two cases is allowed in fluid dynamics. In order to get the correct solution, we should prevent these cases from happening. Hence we do not consider the situation where the point (x_0, y_0) is inside the triangle.

If $\gamma_1 = 0$ or $\gamma_2 = 0$, we can calculate J and I with

$$J(x_0, y_0) = \lim_{(x,y)\to(x_0,y_0)} J(x, y)$$

$$I(x_0, y_0) = \lim_{(x,y)\to(x_0,y_0)} I(x, y)$$

Although $J(x, y)$ and $I(x, y)$ have limits as $(x, y) \to (x_0, y_0)$, it does not guarantee that each term in (12) and (15) will have a finite limit. We will discuss these limits in the next section.

Now we introduce some new quantities and simplify (12) and (15).

$$d_1 \stackrel{def}{=} (c-a)^2 + b^2 \tag{16}$$

$$d_2 \stackrel{def}{=} (c+a)^2 + b^2 \tag{17}$$

$$\xi_1 \stackrel{def}{=} \frac{\beta_1}{b} = \frac{(a-c)(x_0-c) + by_0}{b^2 + (a-c)^2} \tag{18}$$

$$\xi_2 \stackrel{def}{=} \frac{\beta_2}{b} = \frac{(a+c)(x_0+c) + by_0}{b^2 + (a+c)^2} \tag{19}$$

$$\xi_3 \stackrel{def}{=} \frac{(\beta_1 - b)}{b} = \xi_1 - 1 = \frac{(a-c)(x_0-a) + b(y_0-b)}{b^2 + (a-c)^2} \tag{20}$$

$$\xi_4 \stackrel{def}{=} \frac{(\beta_2 - b)}{b} = \xi_2 - 1 = \frac{(a+c)(x_0-a) + b(y_0-b)}{b^2 + (a+c)^2} \tag{21}$$

$$\eta_1 \stackrel{def}{=} \frac{\gamma_1}{b} = \frac{(a-c)y_0 - b(x_0-c)}{b^2 + (a-c)^2} \tag{22}$$

$$\eta_2 \stackrel{def}{=} \frac{\gamma_2}{b} = \frac{(a+c)y_0 - b(x_0+c)}{b^2 + (a+c)^2} \tag{23}$$

$$\eta_3 \stackrel{def}{=} \frac{\gamma_1}{b} = \frac{(a-c)(y_0-b)-b(x_0-a)}{b^2+(a-c)^2} \tag{24}$$

$$\eta_4 \stackrel{def}{=} \frac{\gamma_2}{b} = \frac{(a+c)(y_0-b)-b(x_0-a)}{b^2+(a+c)^2} \tag{25}$$

$$r_1 \stackrel{def}{=} d_2(\xi_2^2+\eta_2^2) = (x_0+c)^2+y_0^2 \tag{26}$$

$$r_2 \stackrel{def}{=} d_1(\xi_1^2+\eta_1^2) = (x_0-c)^2+y_0^2 \tag{27}$$

$$r_3 \stackrel{def}{=} d_1(\xi_3^2+\eta_3^2) = d_2(\xi_4^2+\eta_4^2) = (x_0-a)^2+(y_0-b)^2 \tag{28}$$

Theoretically (22) and (24) are equivalent. $\eta_1 = \eta_3 = \frac{1}{\sqrt{d_1}} \times$ the distance from point Q to line Q_2Q_3. Here we point out that they are two different formulas in the numerical computation. If $Q = (x_0, y_0)$ is near Q_2, (22) is the better way for calculating η_1. However, in the case where Q is close to Q_3, we have to use (24). For (23) and (25), we have a similar situation.

With these notations, (12) and (15) can be written as

$$\begin{aligned} J &= b\left\{\frac{\xi_1}{2}\log\frac{r_3}{r_2} - \frac{\xi_2}{2}\log\frac{r_3}{r_1}\right. \\ &\quad -|\eta_1|\left(\frac{\pi}{2} - \arctan\frac{\eta_1^2+\xi_1^2-\xi_1}{|\eta_1|}\right) \\ &\quad \left. +|\eta_2|\left(\frac{\pi}{2} - \arctan\frac{\eta_2^2+\xi_2^2-\xi_2}{|\eta_2|}\right)\right\} \\ &\stackrel{def}{=} b\left\{J_1+J_2+J_3+J_4\right\} \end{aligned} \tag{29}$$

$$I = b\left\{\frac{\eta_1}{2}\log\frac{r_3}{r_2} - \frac{\eta_2}{2}\log\frac{r_3}{r_1}\right.$$

$$
\begin{aligned}
&+\xi_1 \mathrm{sign}(\eta_1)\left(\frac{\pi}{2} - \arctan\frac{\eta_1^2+\xi_1^2-\xi_1}{|\eta_1|}\right) \\
&\quad -\xi_2 \mathrm{sign}(\eta_2)\left(\frac{\pi}{2} - \arctan\frac{\eta_2^2+\xi_2^2-\xi_2}{|\eta_2|}\right)\Bigg\} \qquad (30) \\
&\stackrel{def}{=} b\left\{I_1+I_2+I_3+I_4\right\}
\end{aligned}
$$

(29) and (30) are the mathematical formulas for the velocity induced by a triangle. In the case where they behave well numerically, we use them directly in the calculation. In the other cases, numerical cancellation may cause a loss of accuracy and we have to change them into forms which have good numerical performance. We discuss this in the next section.

2 Numerical singularity and the way to avoid it

Now let us examine J_1 in (29) and I_3 in (30) in the limit $Q \to Q_3$.

As $Q = (x_0, y_0) \to Q_3$, we have $r_3 \to 0$, $\eta_1 \to 0$, $r_2 \to d_1$, $\xi_1 \to 1$,

$$
\begin{aligned}
&\lim_{Q\to Q_3} J_1 = \lim_{Q\to Q_3} \frac{\xi_1}{2}\log\frac{r_3}{r_2} = \infty \\
&\lim_{Q\to Q_3} I_3 = \lim_{Q\to Q_3} \xi_1 \mathrm{sign}(\eta_1)\left(\frac{\pi}{2} - \arctan\frac{\eta_1^2+\xi_1^2-\xi_1}{|\eta_1|}\right) \quad \text{does not exist}
\end{aligned}
$$

The fact that J_1 and I_3 have a singularity at Q_3 does not necessarily imply that J and I have a singularity at Q_3. In fact, as we will find later in this section, $J(x_0, y_0)$ and $I(x_0, y_0)$ do have finite limits as $Q = (x_0, y_0) \to Q_3$. The singularity of J_1 and I_3 at Q_3 tells us that the numerical expression

for J and I should take a form other than (29) and (30) if $Q = (x_0, y_0)$ is close to Q_3. The purpose is to avoid numerical cancellation. The situation here is very similar to the following example.

Suppose we calculate $f(x)$ with the following two expressions.

$$f(x) = \sqrt{x + x^2} - x \tag{31}$$

$$\text{and} \quad f(x) = \frac{x}{\sqrt{x + x^2} + x} \tag{32}$$

When x is positively large, to get a numerical result with small relative error, we have to use (32). However, if x is negatively large, (31) is preferred.

In this section, we will write (29) and (30) in different forms. Mathematically, all these forms are equivalent. Numerically, different forms are used for different situations. For each situation, we choose a suitable form such that no term in that form has a singularity. As explained in Section 1, we always assume $Q = (x_0, y_0)$ is not inside the triangle.

Case 1: $r_3 > \frac{1}{4}\min\{d_1, d_2\}$ and $\sqrt{x_0^2 + y_0^2} < 6c$.

We use (29) and (30) for J and I respectively.

In the limit $Q \to Q_2$, J_1, J_3, I_1 and I_3 all go to zero.

$$\lim_{Q \to Q_2} J_1 = \lim_{Q \to Q_2} \frac{\xi_1}{2} \log \frac{r_3}{r_2} = 0$$

$$\lim_{Q \to Q_2} J_3 = \lim_{Q \to Q_2} -|\eta_1| \left(\frac{\pi}{2} - \arctan \frac{\eta_1^2 + \xi_1^2 - \xi_1}{|\eta_1|} \right) = 0$$

$$\lim_{Q\to Q_2} I_1 = \lim_{Q\to Q_2} \frac{\eta_1}{2}\log\frac{r_3}{r_2} = 0$$

$$\lim_{Q\to Q_2} I_3 = \lim_{Q\to Q_2} \xi_1 \mathrm{sign}(\eta_1)\left(\frac{\pi}{2} - \arctan\frac{\eta_1^2+\xi_1^2-\xi_1}{|\eta_1|}\right) = 0$$

As a matter of fact, none of J_1, J_2, J_3, J_4 in (29) and I_1, I_2, I_3, I_4 in (30) has a singularity as $Q = (x_0, y_0) \to Q_2$

The same statement holds as $Q = (x_0, y_0) \to Q_1$.

Case 2: $r_3 \le \frac{1}{4}\min\{d_1, d_2\}$.

As $Q = (x_0, y_0) \to Q_3$, we have $\eta_1 \to 0$, $\eta_2 \to 0$, $\xi_1 \to 1$, $\xi_2 \to 1$.

$$\lim_{Q\to Q_3} I_3 \text{ does not exist}, \quad \lim_{Q\to Q_3} I_4 \text{ does not exist}$$

$$\lim_{Q\to Q_3} (I_3 + I_4) = -\Theta$$

$$\Theta = \begin{cases} \angle(QQ_1, QQ_2) & \text{if } Q \text{ and } Q_3 \text{ are on the same side of } Q_1Q_2 \\ -\angle(QQ_1, QQ_2) & \text{if } Q \text{ and } Q_3 \text{ are on different sides of } Q_1Q_2 \end{cases}$$

where $\angle(QQ_1, QQ_2)$ is the angle spanned by vector $Q\bar{Q}_1$ and vector $Q\bar{Q}_2$, which falls in $[0, \pi]$.

If we first calculate I_3 and I_4, then add them together, the large errors occurred in the calculations of I_3 and I_4 will destroy the accuracy of (I_3+I_4).

To evaluate $I_3 + I_4$ numerically, we write it in the following form

$$\begin{aligned} I_3 + I_4 &= \xi_3 \mathrm{sign}(\eta_3)\left(\frac{\pi}{2} - \arctan\frac{\eta_3^2+\xi_3^2+\xi_3}{|\eta_3|}\right) \\ &\quad -\xi_4 \mathrm{sign}(\eta_4)\left(\frac{\pi}{2} - \arctan\frac{\eta_4^2+\xi_4^2+\xi_4}{|\eta_4|}\right) - \Theta \end{aligned}$$

Hence, in this case, we use the following expression for I.

$$
\begin{aligned}
I &= b\left\{\frac{\eta_3}{2}\log\frac{r_3}{r_2} - \frac{\eta_4}{2}\log\frac{r_3}{r_1}\right. \\
&\quad +\xi_3\mathrm{sign}(\eta_3)\left(\frac{\pi}{2} - \arctan\frac{\eta_3^2+\xi_3^2+\xi_3}{|\eta_3|}\right) \\
&\quad \left. - \xi_4\mathrm{sign}(\eta_4)\left(\frac{\pi}{2} - \arctan\frac{\eta_4^2+\xi_4^2+\xi_4}{|\eta_4|}\right) - \Theta\right\} \qquad (33) \\
&\stackrel{def}{=} b\left\{I_5 + I_6 + I_7 + I_8 + I_9\right\}
\end{aligned}
$$

For J, we use

$$
\begin{aligned}
J &= b\left\{\frac{\xi_3}{2}\log\frac{r_3}{r_2} - \frac{\xi_4}{2}\log\frac{r_3}{r_1} + \frac{1}{2}\log\frac{r_1}{r_2}\right. \\
&\quad -|\eta_3|\left(\frac{\pi}{2} - \arctan\frac{\eta_3^2+\xi_3^2+\xi_3}{|\eta_3|}\right) \\
&\quad \left. +|\eta_4|\left(\frac{\pi}{2} - \arctan\frac{\eta_4^2+\xi_4^2+\xi_4}{|\eta_4|}\right)\right\} \qquad (34) \\
&\stackrel{def}{=} b\left\{J_5 + J_6 + J_7 + J_8 + J_9\right\}
\end{aligned}
$$

We checked the behavior of every term in (33) and (34). No term has a singularity as $Q = (x_0, y_0) \to Q_3$.

Case 3: $\sqrt{x_0^2 + y_0^2} > 6c$.

First let us point out the problem (29) has when $x_0^2 + y_0^2$ is large.

When $y_0 = 0$ and $x_0 \to \infty$, we have

$$
\lim_{\substack{x_0=0 \\ y_0\to\infty}} J_1 = \lim_{\substack{x_0=0 \\ y_0\to\infty}} \frac{\xi_1}{2}\log\frac{r_3}{r_2} = \frac{-b^2}{b^2+(a-c)^2} \neq 0
$$

$$\lim_{\substack{x_0=0\\ y_0\to\infty}} J_2 = \frac{b^2}{b^2+(a+c)^2} \neq 0$$

$$\lim_{\substack{x_0=0\\ y_0\to\infty}} J_3 = \frac{-(a-c)^2}{b^2+(a-c)^2} \neq 0$$

$$\lim_{\substack{x_0=0\\ y_0\to\infty}} J_4 = \frac{(a+c)^2}{b^2+(a+c)^2} \neq 0$$

There is no singularity in J_1, J_2, J_3 and J_4. However, while J_1, J_2, J_3 and J_4 all tend to nonzero values in the limit $Q \to \infty$, their sum goes to zero:

$$\lim_{\substack{x_0=0\\ y_0\to\infty}} J = \lim_{\substack{x_0=0\\ y_0\to\infty}} b\left\{J_1+J_2+J_3+J_4\right\} = 0$$

Generally speaking, if J is computed using (29), the magnitude of the absolute error in J is about the same order as those in J_1, J_2, J_3 and J_4. Consequently the absolute error in J will not tend to zero while J itself goes to zero. This leads to a large relative error for J. To calculate the velocity at points far from the triangle, we need to change (29) into a form in which every term vanishes as $Q \to \infty$.

As $r = \sqrt{x_0^2+y_0^2} \to \infty$, J is of the order $O(r^{-1})$. We now find a form for J such that all terms in it behave like $O(r^{-1})$.

$$\begin{aligned} J = b\Bigg\{ & \frac{\xi_1}{2}\log\frac{r_3}{r_2} - \frac{\xi_2}{2}\log\frac{r_3}{r_1} \\ & -|\eta_1|\left(\frac{\pi}{2} - \arctan\frac{\eta_1^2+\xi_1^2-\xi_1}{|\eta_1|}\right) \\ & +|\eta_2|\left(\frac{\pi}{2} - \arctan\frac{\eta_2^2+\xi_2^2-\xi_2}{|\eta_2|}\right)\Bigg\} \end{aligned}$$

$$
\begin{aligned}
&= b\left\{\frac{\xi_1}{2}\left[\log\frac{(1-\xi_1)^2+\eta_1^2}{\xi_1^2+\eta_1^2}+\frac{2\xi_1}{\xi_1^2+\eta_1^2}\right]\right.\\
&\quad -\frac{\xi_2}{2}\left[\log\frac{(1-\xi_2)^2+\eta_2^2}{\xi_2^2+\eta_2^2}+\frac{2\xi_2}{\xi_2^2+\eta_2^2}\right]\\
&\quad -|\eta_1|\left[\arctan\frac{|\eta_1|}{\eta_1^2+\xi_1^2-\xi_1}-\frac{|\eta_1|}{\xi_1^2+\eta_1^2}\right]\\
&\quad \left.|\eta_2|\left[\arctan\frac{|\eta_2|}{\eta_2^2+\xi_2^2-\xi_2}-\frac{|\eta_2|}{\xi_2^2+\eta_2^2}\right]\right\}\\
&= b\left\{\frac{\xi_1}{2}\left[F\left(\frac{\xi_1-1/2}{\xi_1^2+\eta_1^2-\xi_1+1/2}\right)+A_1\right]\right.\\
&\quad -\frac{\xi_2}{2}\left[F\left(\frac{\xi_2-1/2}{\xi_2^2+\eta_2^2-\xi_2+1/2}\right)+A_2\right]\\
&\quad -|\eta_1|\left[G\left(\frac{|\eta_1|}{\eta_1^2+\xi_1^2-\xi_1}\right)+B_1\right]\\
&\quad \left.+|\eta_2|\left[G\left(\frac{|\eta_2|}{\eta_2^2+\xi_2^2-\xi_2}\right)+B_2\right]\right\} \qquad (35)\\
&\stackrel{def}{=} b\left\{J_{10}+J_{11}+J_{12}+J_{13}\right\}
\end{aligned}
$$

where the functions F and G are defined as

$$F(s) = \log\frac{(1-s)}{(1+s)} + 2s \qquad (36)$$

$$G(s) = \arctan(s) - s \qquad (37)$$

and A_1, A_2, B_1 and B_2 are

$$
\begin{aligned}
A_1 &= \frac{\eta_1^2-\xi_1^2+\xi_1}{(\xi_1^2+\eta_1^2-\xi_1+1/2)(\xi_1^2+\eta_1^2)}\\
A_2 &= \frac{\eta_2^2-\xi_2^2+\xi_2}{(\xi_2^2+\eta_2^2-\xi_2+1/2)(\xi_2^2+\eta_2^2)}\\
B_1 &= \frac{\xi_1|\eta_1|}{(\eta_1^2+\xi_1^2-\xi_1)(\xi_1^2+\eta_1^2)}\\
B_2 &= \frac{\xi_2|\eta_2|}{(\eta_2^2+\xi_2^2-\xi_2)(\xi_2^2+\eta_2^2)}
\end{aligned}
$$

For I, we have

$$
\begin{aligned}
I &= b\left\{\frac{\eta_1}{2}\left[F\left(\frac{\xi_1-1/2}{\xi_1^2+\eta_1^2-\xi_1+1/2}\right)+A_1\right]\right. \\
&\quad -\frac{\eta_2}{2}\left[F\left(\frac{\xi_2-1/2}{\xi_2^2+\eta_2^2-\xi_2+1/2}\right)+A_2\right] \\
&\quad +\xi_1\mathrm{sign}(\eta_1)\left[G\left(\frac{|\eta_1|}{\eta_1^2+\xi_1^2-\xi_1}\right)+B_1\right] \\
&\quad \left.-\xi_2\mathrm{sign}(\eta_2)\left[G\left(\frac{|\eta_2|}{\eta_2^2+\xi_2^2-\xi_2}\right)+B_2\right]\right\} \qquad (38) \\
&\stackrel{def}{=} b\left\{I_{10}+I_{11}+I_{12}+I_{13}\right\}
\end{aligned}
$$

Although all terms in (35) and (38) tend to zero as $x_0^2+y_0^2\to\infty$, we may still suffer from numerical cancellation when calculating F and G. To avoid loss of accuracy, we expand F and G into power series:

$$
\begin{aligned}
F(s) &= \log\frac{(1-s)}{(1+s)}+2s \\
&= -2s^3\left(\frac{1}{3}+\sum_{i=1}^{8}\frac{1}{2i+3}s^{2i}+\epsilon_1(s)\right) \qquad (39) \\
&\qquad |\epsilon_1(s)|<10^{-16} \quad \text{when } |s|<0.15
\end{aligned}
$$

$$
\begin{aligned}
G(s) &= \arctan(s)-s \\
&= -s^3\left(\frac{1}{3}+\sum_{i=1}^{8}\frac{(-1)^i}{2i+3}s^{2i}+\epsilon_2(s)\right) \qquad (40) \\
&\qquad |\epsilon_2(s)|<10^{-16} \quad \text{when } |s|<0.15
\end{aligned}
$$

As $r=\sqrt{x_0^2+y_0^2}\to\infty$, the functions F and G are of the order $O(r^{-3})$, and A_1, A_2, B_1 and B_2 are of the order $O(r^{-2})$. It follows immediately that all terms in (35) and (38) are of the order $O(r^{-1})$.

Finally, it should be pointed out that, in programming, I and J are not difficult to calculate.

3 The numerical method

To obtain the fluid velocity, we do two things:

1. Approximate the boundary curve of each patch Ω_i by interpolation.

2. Evaluate the integrals of the kernel on Ω_i in (7) and (8).

In our method, the boundary of each patch is numerically represented by the nodes distributed along it. The curves between adjacent nodes are approximately determined with the second-order interpolation. Suppose Q_j and Q_{j+1} are two adjacent nodes. To approximate the curve between Q_j and Q_{j+1}, we establish a local coordinate system, taking the line Q_jQ_{j+1} as x-axis and the perpendicular bisector of Q_jQ_{j+1} as y-axis. For the simplicity of the interpolation here and the integration later, we let the interpolation curve be a parabola with $y-$axis as its line of symmetry. The equation for the parabola is

$$y = h_j \left[1 - \left(\frac{x}{l_j}\right)^2\right] \quad \text{for} \quad -l_j \leq x \leq l_j$$

where l_j is one half of the distance between Q_j and Q_{j+1}, and h_j is the height of the parabola which is determined by the points Q_{j-1}, Q_j, Q_{j+1} and Q_{j+2} with the following formulas.

$$
\begin{aligned}
l_j &= \frac{1}{2}\sqrt{(x_{j+1}-x_j)^2+(y_{j+1}-y_j)^2} \\
\vec{\rho_{j+\frac{1}{2}}} &= \vec{Q_jQ_{j+1}} = \frac{1}{2l_j}[(x_{j+1}-x_j),(y_{j+1}-y_j)] \\
\vec{\rho_j} &= \frac{l_j}{l_{j-1}+l_j}\vec{\rho_{j-\frac{1}{2}}} + \frac{l_{j-1}}{l_{j-1}+l_j}\vec{\rho_{j+\frac{1}{2}}} \\
\alpha_j &= \frac{1}{2}\left|\vec{\rho_{j+1}}-\vec{\rho_j}\right| \\
h_j &= l_j\frac{\alpha_j}{1+\sqrt{1-\alpha_j^2}}
\end{aligned}
$$

Suppose $\tilde{\Omega}$ is the region enclosed by these interpolation curves. Then $\tilde{\Omega}$ is a third order approximation of the real patch region Ω if the boundary of Ω is smooth. Although we can describe the boundary more accurately by using higher-order interpolation, it will not reduce the total numerical error if we cannot evaluate the integrals on $\tilde{\Omega}$ in (7) and (8) to the same high order accuracy.

A patch $\tilde{\Omega}$ has two parts $\tilde{\Omega} = \tilde{P}+\tilde{R}$. $\tilde{P}$ is the polygon with the numerical nodes as its vertices. $\tilde{R}$ is the residual part. Thus the integrals on $\tilde{\Omega}_i$ in (7) and (8) can be written as

$$\int_{\tilde{\Omega}_i(t)} = \int_{\tilde{P}_i(t)} + \int_{\tilde{R}_i(t)} \tag{41}$$

We then cut the polygon $\tilde{P}_i(t)$ into triangles. In Section 1 and 2, we derived and discussed the numerical formula for the velocity induced by a triangle. The integrals on $\tilde{P}_i(t)$ in (41) can be easily obtained by summing the contributions of all triangles. $\tilde{R}_i(t)$ consists of a lot of lens-shaped areas. Each one is an area enclosed by a parabola and a straight line. $\tilde{R}_i(t)$ has a very small area and the integrals on $\tilde{R}_i(t)$ in (41) are of the order $(\sim O(\triangle s)^2)$. To obtain third-order accuracy in space dimensions, we only need a first-order approximation of the velocity induced by $\tilde{R}_i(t)$.

We approximate a lens-shaped vortex area by a vortex sheet, i.e. we imagine that the vorticity in a lens-shaped area is concentrated along its bottom. The distribution of vorticity along the sheet is given by

$$e_j(x) = \omega h_j \left[1 - \left(\frac{x}{l_j}\right)^2\right] \quad \text{for} \quad -l_j \le x \le l_j$$

The velocity induced by a vortex sheet of this kind is given by

$$\begin{aligned} u(x_0, y_0) &= \frac{1}{2\pi}\int_{-l}^{l} e(x)\frac{-y_0}{(x-x_0)^2+y_0^2}dx \\ &= \frac{\omega}{2\pi}h\int_{-1}^{1}(1-\sigma^2)\frac{-\tau_0}{(\sigma-\sigma_0)^2+\tau^2}d\sigma \stackrel{def}{=} \frac{\omega h}{2\pi}K \\ v(x_0, y_0) &= \frac{1}{2\pi}\int_{-l}^{l} e(x)\frac{(x_0-x)}{(x-x_0)^2+y_0^2}dx \\ &= \frac{\omega}{2\pi}h\int_{-1}^{1}(1-\sigma^2)\frac{(\sigma_0-\sigma)}{(\sigma-\sigma_0)^2+\tau^2}d\sigma \stackrel{def}{=} \frac{\omega h}{2\pi}L \end{aligned}$$

where

$$\sigma_0 = \frac{x_0}{l}, \qquad \tau_0 = \frac{y_0}{l}$$

A little algebra shows that

$$\begin{aligned} L = 2\sigma_0 &+ \frac{(\sigma_0 - 1)(\sigma_0 + 1) - \tau_0^2}{2} \log \frac{(\sigma_0 - 1)^2 + \tau_0^2}{(\sigma_0 + 1)^2 + \tau_0^2} \\ &-2\sigma_0\tau_0 \left(\frac{\pi}{2} - \arctan \frac{\sigma_0^2 + \tau_0^2 - 1}{2\tau_0} \right) \end{aligned} \tag{42}$$

$$\begin{aligned} K = 2\tau_0 &+ \tau_0\sigma_0 \log \frac{(\sigma_0 - 1)^2 + \tau_0^2}{(\sigma_0 + 1)^2 + \tau_0^2} \\ &+ \left[(\sigma_0 - 1)(\sigma_0 + 1) - \tau_0^2\right] \left(\frac{\pi}{2} - \arctan \frac{\sigma_0^2 + \tau_0^2 - 1}{2\tau_0} \right) \end{aligned} \tag{43}$$

Similar to the situation in section 2, here we must change the numerical formulas, (42) and (43), into a different form when $\sigma_0^2 + \tau_0^2$ is large. Again the purpose is to avoid numerical cancellation.

For $\sqrt{\sigma_0^2 + \tau_0^2} > 6$, we use the following expressions for L and K.

$$\begin{aligned} L = &\frac{4\sigma_0(\sigma_0^2 - \tau_0^2 - 1)}{(\sigma_0^2 + \tau_0^2 + 1)(\sigma_0^2 + \tau_0^2 - 1)} \\ &+ \frac{(\sigma_0^2 - \tau_0^2 - 1)}{2} \left[F\left(\frac{2\sigma_0}{\sigma_0^2 + \tau_0^2 + 1} \right) \right] \\ &-2\sigma_0\tau_0 \left[G\left(\frac{2\tau_0}{\sigma_0^2 + \tau_0^2 - 1} \right) \right] \end{aligned} \tag{44}$$

$$\begin{aligned} K = &\frac{4\tau_0(\sigma_0^2 - \tau_0^2 - 1)}{(\sigma_0^2 + \tau_0^2 + 1)(\sigma_0^2 + \tau_0^2 - 1)} \\ &+\tau_0\sigma_0 \left[F\left(\frac{2\sigma_0}{\sigma_0^2 + \tau_0^2 + 1} \right) \right] \\ &+(\sigma_0^2 - \tau_0^2 - 1) \left[G\left(\frac{2\tau_0}{\sigma_0^2 + \tau_0^2 - 1} \right) \right] \end{aligned} \tag{45}$$

where F and G are the same functions as defined by (36) and (37). As $r = \sqrt{\sigma_0^2 + \tau_0^2} \to \infty$, the functions F and G are of the order $O(r^{-3})$. Consequently all terms in (44) and (45) are of the order $O(r^{-1})$. This conforms to the fact that the velocity is of the order $O(r^{-1})$. Hence (44) and (45) are the appropriate formulas for numerical calculation when $\sigma_0^2 + \tau_0^2$ is large.

Summing the contributions of these vortex sheets, we get a first-order approximation of the integrals on $\tilde{R}_i(t)$ in (41). Therefore, $\int_{\tilde{\Omega}_i}$, the left hand side of (41), can be evaluated with third-order accuracy.

Finally, summing the contributions of all vortex patches yields the total fluid velocity $\vec{u}(x_0, y_0, t) = [u(x_0, y_0, t), v(x_0, y_0, t)]$.

Once we know the total fluid velocity, we integrate in time using a fourth-order Runge-Kutta method [9].

Initially, we distribute numerical nodes along the boundaries of the patches according to the following rules:

1. The distance between adjacent nodes is less than a specified Δs :

$$|Q_j Q_{j+1}| < \Delta s$$

2. Twice the angle between vector $\vec{Q_j Q_{j+\frac{1}{2}}}$ and vector $\vec{Q_{j+\frac{1}{2}} Q_{j+1}}$ is less than a specified $\Delta\theta$: $\quad 2|\angle(Q_j Q_{j+\frac{1}{2}}, Q_{j+\frac{1}{2}} Q_{j+1})| < \Delta\theta$

3. Either $|Q_jQ_{j+1}| > \frac{1}{2}\Delta s$ or $2|\angle(Q_jQ_{j+\frac{1}{2}}, Q_{j+\frac{1}{2}}Q_{j+1})| > \frac{1}{2}\Delta\theta$, or both of them are satisfied.

Here $Q_{j+\frac{1}{2}}$ is the vertex of the interpolation parabola between Q_j and Q_{j+1}. In the above three rules, rule 1 prevents a loss of information about the curve between adjacent nodes, rule 2 provides a fine local representation where the boundary has large curvature, and rule 3 guarantees that we do not have redundant nodes.

During the evolving of the patches, some parts of the boundaries will be stretched and the curvature of some parts will increase. In order to maintain the resolution of the boundaries and keep the method efficient, it is necessary to add and delete nodes.

When $|Q_jQ_{j+1}| > \sqrt{2}\Delta s$ or $2|\angle(Q_jQ_{j+\frac{1}{2}}, Q_{j+\frac{1}{2}}Q_{j+1})| > \sqrt{2}\Delta\theta$, we add $Q_{j+\frac{1}{2}}$ as a new node between Q_j and Q_{j+1}.

When $|Q_{j-1}Q_{j+1}| < \Delta s$ and $2|\angle(Q_{j-1}Q_j, Q_jQ_{j+1})| < \Delta\theta$, we simply drop the node Q_i.

In our method, a patch with n numerical nodes along it, is approximated by n lens-shaped areas and an n-sided polygon which is then decomposed into $(n-2)$ triangles. The total number of the elements (triangles and lens-shaped areas) is less than $2N$, where N is the total number of the nodes

along all patches. The amount of work required to advance the patches for a single time step is of the order $O(N^2)$ which is generic for vortex methods if fast summation is not used. In the next section, we show that the method is third order accurate in space dimensions.

4 Error analysis

Now we discuss the numerical error of the method. There are two sources of error in the method: the error associated with the approximation of the fluid velocity, and the error associated with the time integration. The error from the fourth order Runge-Kutta time integration should be fourth-order and we will not discuss it here. The error from the approximation of the velocity can be broken into two parts. The first part of the error is due to the fact that a patch Ω is represented by a finite number of nodes. The boundary of the patch can not be fully recovered from these finite nodes. The new patch $\tilde{\Omega}$, formed by the interpolation curves, is used to approximate the real patch Ω. Geometrically, $\tilde{\Omega}$ is a third order approximation of Ω. Later, we will show that the difference between the velocities induced by Ω and $\tilde{\Omega}$ can be bounded by $O((\triangle s)^3|\log \triangle s|)$. The approximate patch $\tilde{\Omega}$ is the union of a polygon and a residual part. The second part of the error is due to

the fact that we do not have an exact velocity formula for the residual part. Instead, we approximate each lens-shaped vortex area in the residual part by a vortex sheet. This error is also bounded by $O((\triangle s)^3|\log \triangle s|)$.

In fact, the numerical error also depends on the stability of the physical problem. Since such stability is a very complicated issue, we are not going to say anything about it. Here we only give an estimate of the numerical error in a single time step.

Suppose $U(x_0, y_0)$ is the velocity induced by the patch Ω, $U_1(x_0, y_0)$ is the velocity induced by the approximate patch $\tilde{\Omega}$, and $U_2(x_0, y_0)$ is the velocity induced by the polygon plus the vortex sheets which are used to approximate $\tilde{\Omega}$. We see that $U(x_0, y_0)$ is the exact velocity and $U_2(x_0, y_0)$ is the velocity we use in the numerical method. The spatial error E_s is

$$E_s = \max_{(x_0,y_0)} |U(x_0, y_0) - U_2(x_0, y_0)|$$

Now we try to bound $|U(x_0, y_0) - U_2(x_0, y_0)|$. First we have

$$|U(x_0, y_0) - U_2(x_0, y_0)| \leq |U(x_0, y_0) - U_1(x_0, y_0)| + |U_1(x_0, y_0) - U_2(x_0, y_0)|$$

$$\text{and} \qquad |U(x_0, y_0) - U_1(x_0, y_0)| \leq C_1 \int_{\triangle\Omega} \frac{1}{r} dxdy \tag{46}$$

where $r = \sqrt{(x - x_0)^2 + (y - y_0)^2}$, and $\triangle\Omega = (\Omega\backslash\tilde{\Omega})\cup(\tilde{\Omega}\backslash\Omega)$ is the difference between Ω and $\tilde{\Omega}$. Assume that the patch Ω is contained in $B(0, R)$ which

is the ball centered at the origin with radius R, and that its boundary $\partial\Omega$ is smooth enough. It follows that $\triangle\Omega$ can be covered by a strip along the boundary $\partial\Omega$

$$\triangle\Omega \subset S = \left\{(x,y)\middle|\sqrt{(x-\xi)^2+(y-\eta)^2} < \frac{d}{2} \quad \text{for some}(\xi,\eta) \in \partial\Omega\right\}$$

where $d \sim O(\triangle s)^3$.

If (x_0, y_0) is inside $B(0, 2R)$, we find

$$\begin{aligned}
&|U(x_0,y_0) - U_1(x_0,y_0)| \leq C_1 \int_S \frac{1}{r} dxdy \\
&\leq C_1 \left\{ \int_{B((x_0,y_0),d)} \frac{1}{r} dxdy + \int_{S\setminus B((x_0,y_0),d)} \frac{1}{r} dxdy \right\} \\
&\leq C_2 \cdot d + C_1 \int_d^{3R} \frac{1}{r} dA(r) \qquad (47)
\end{aligned}$$

where $A(r)$ is the area of $S \cap B((x_0, y_0), r)$. Integrating by parts, we get

$$\int_d^{3R} \frac{1}{r} dA(r) = \frac{A(3R)}{3R} - \frac{A(d)}{d} + \int_d^{3R} A(r) \frac{1}{r^2} dr \qquad (48)$$

We further assume that the length of the intersection of $\partial\Omega$ and a ball can be bounded by a constant times the radius of the ball. That is, there exists a constant M such that for any point $\alpha = (x, y)$ and any number $r > 0$, Length of $\partial\Omega \cap B(\alpha, r) < M \cdot r$. With this assumption, we have

$$A(r) < 2Mrd \qquad (49)$$

Combining Eqn(49), Eqn(48) and Eqn(47), we get

$$\int_S \frac{1}{r} dxdy < C_3 d + \int_d^{3R} \frac{2Md}{r} dr$$
$$= C_4 d(1 + |\log d|)$$

If (x_0, y_0) is outside $B(0, 2R)$, $\int_S \frac{1}{r} dxdy$ can be easily bounded by the area of the strip S :

$$\int_S \frac{1}{r} dxdy < \frac{1}{R} Area(S) < 2Md$$

In both cases, we have

$$|U(x_0, y_0) - U_1(x_0, y_0)| \leq Cd(1 + |\log d|)$$
$$= O(\triangle s)^3(|\log \triangle s|)$$

With the above assumptions, it is also true that

$$|U_1(x_0, y_0) - U_2(x_0, y_0)| = O(\triangle s)^3(|\log \triangle s|)$$

Thus we obtain

$$|U(x_0, y_0) - U_2(x_0, y_0)| = O(\triangle s)^3(|\log \triangle s|)$$

In the above, the smoothness of $\partial\Omega$ is only used to determine the width of $\triangle\Omega$. We have not made any use of the particular shape of $\triangle\Omega$. Eqn(46) is also a very rough estimate. Based on the analysis in some very simple

cases, we believe that the real bound for $|U(x_0, y_0) - U_2(x_0, y_0)|$ should be $O(\triangle s)^3$, but we are not able to prove it here.

We expect the total numerical error to be of the form

$$Error \simeq C(\triangle s)^3 + D(\triangle t)^4 \tag{50}$$

To demonstrate the validity of Eqn(50) numerically, we compare the exact solution for an elliptical patch given by Lamb [10] with the numerical solutions obtained by our method. Consider an ellipse with $a = 2$, $b = 1$, where a and b are the lengths of the semi-major and semi-minor axes of the ellipse, respectively. The numerical experiments were carried out with $\omega = 1$. The $Error$ is defined as the maximum difference between the exact solution and the numerical solution. We find that the $Error$ satisfies Eqn(50) approximately with $C = 0.063T$ and $D = 0.0008T$, where T is the time. Of course, this is a simple problem in which the vortex patch, while rotating, always remains of the same elliptical shape. For the general problem, we believe Eqn(50) is still true, but the coefficients C and D may not depend linearly on the time T.

5 Numerical experiments

In this section, we will display some numerical results obtained using the method described above.

Example 1:

As shown in Fig.2, initially two circular vortex patches with unit radius are located along y-axis and are separated by a distance of 0.1. The patch at top has vorticity of 2.0 and the patch at bottom has vorticity of 1.0 [3]. The numerical computations were carried out with $\Delta s = \frac{2\pi}{64}$, $\Delta\theta = \frac{2\pi}{64}$ and $\Delta t = 0.2$. At $t = 0$ we distribute 128 nodes uniformly to approximate the boundaries of two patches, 64 nodes for each patch. At $t = 14.0$, there are 427+327=754 numerical nodes approximating the boundaries. Fig.2-Fig.4 show the configurations of the patches at different times. The whole calculation took about 30 hours on a SUN 3/50. We choose this problem to show the generic structures which evolve in patches of constant vorticity. The long narrow structures in Fig.4 are typical of the structures in vortex patch problems. With its sides approaching each other, the long thin arm in Fig.4 contains a very small fraction of the total area of the patch, whereas it contains a large fraction of the perimeter of the patch. In our method, the fluid velocity is calculated by integrating a kernel on the region of the

patches, instead of along the boundaries. Although the kernel is singular, its integral on each element (triangle or sheet) is not. Thus our method can resolve the long and thin features without loss of accuracy. Our computation can be continued up to $t = 16.0$. At that time, the thin structure is so narrow that the two polylines along its two sides intersect each other. Linking the numerical nodes sequentially no longer forms a regular polygon. We can reduce $\triangle s$ to continue the calculation.

Example 2:

Initially two identical circular vortex patches are located along y-axis. They are circles of radius 1.0 and are separated by a distance of 0.5. Both of the patches have vorticity equal to 1.0 [4]. At the beginning, we did the numerical simulation with $\Delta s = \frac{2\pi}{64}$, $\Delta\theta = \frac{2\pi}{64}$ and $\Delta t = 0.1$. Fig.5 shows the configuration of the patches at T=24.0. From the numerical result, we see that, along the boundary of each patch, there is a region with large positive curvature, while the curvature remains negative and small on either side of the region. We call it Region A . Previously, whether or not there is a singularity was discussed in [4, 5, 6, 7]. Since a lot of numerical nodes are added by second order interpolation during the calculation, it may introduce some smoothing in our method. In order to investigate whether there

is a singularity, we make sure that we are not smoothing the boundaries artificially. We carry out the simulations in the following way. First we run the calculation and find out the Lagrangian coordinate of Region A (initial arclength from a reference point to Region A). Then we carry out the calculation again. During this calculation, we write down the Lagrangian coordinates of the numerical nodes that have ever been added near Region A , and we do not delete any node near Region A . Once we know their Lagrangian coordinates, we distribute these nodes initially (at $t = 0$) along the boundary and do the calculation the third time. The purpose is to make sure that there is no need to add new nodes near Region A in the third calculation. Comparing the numerical results obtained by the first run and the third run, we find that they are almost identical. This indicates that, in fact, the second order interpolation for adding new points introduces no artificial smoothing. Fig.6 shows the fine details of the boundary near Region A. Now it seems to us that Region A is a region with large curvature instead of a singularity. To determine whether Region A is a singularity or not, we study the behavior of the curvature near Region A in the limit $\triangle t \to 0$ and $\triangle s \to 0$. Fig.7 shows the curvature near Region A for $\triangle t = 0.1$, $\triangle t = 0.05$ and $\triangle t = 0.025$ with $\triangle s = \frac{2\pi}{64}$. Fig.8 shows the curvature near

Region A for $\triangle s = \frac{2\pi}{64}$, $\triangle s = \frac{2\pi}{128}$ and $\triangle s = \frac{2\pi}{256}$ with $\triangle t = 0.1$. Our method has a third order accuracy for the positions of the numerical nodes along the boundaries. Generally, we can only expect a first order accuracy for the curvature obtained from the numerical solution, since the curvature involves the second order derivatives of the boundary curve. For a second order method, it will not be easy to calculate the curvature from the numerical solution. In Fig.7, the variation of curvature for different $\triangle t$'s is less than 0.05%, which is not distinguishable. In Fig.8, the difference between curvatures for $\triangle s = \frac{2\pi}{64}$ and $\triangle s = \frac{2\pi}{128}$ is less than 4%, and the difference between curvatures for $\triangle s = \frac{2\pi}{128}$ and $\triangle s = \frac{2\pi}{256}$ is less than 0.02%. Based on these facts, we believe that the curvature in Region A converges as $\triangle t \to 0$ and $\triangle s \to 0$, and it converges to a finite value. The maximum curvature in Region A is 22.50.

Conclusion

We have presented a high order numerical method for simulating the evolution of patches of constant vorticity. It has a third-order accuracy in space dimensions when the boundary curves are smooth. Because of its high-order accuracy, we are able to get numerical solutions of higher resolution with

fewer numerical nodes. Since the cost is proportional to the square of the number of numerical nodes, our method has the advantage when we want a very accurate numerical solution, especially when we want to study the details of the boundaries. Also in our method, numerical cancellation has been carefully avoided, so accuracy does not degrade as the boundaries are stretched and long thin finger structures form. As an example, we studied the problem of two identical circular vortex patches initially separated by a distance of half their radius. We showed numerically that, as we refine $\triangle t$ and $\triangle s$, the numerical representation of the boundary does converge and converges to a smooth curve.

Acknowledgement

I would like to thank Professor Alexandre Joel Chorin for his guidance, support and encouragement.

References

[1] A. J. CHORIN, Numerical study of slightly viscous flow, *J. Fluid Mech.*, Vol. 57, 785-796 (1973).

[2] N. J. ZABUSKY, M. H. HUGHES, AND K. V. ROBERTS, Contour dynamics for the Euler equations in two dimensions, *J. Comput. Phys.* Vol. 30, 96 (1979).

[3] T. F. BUTTKE, A fast adaptive vortex method for patches of constant vorticity in two dimensions, *J. Comput. Phys.* Vol. 89, 161 (1990).

[4] T. F. BUTTKE, The observation of singularities in the boundary of patches of constant vorticity, *Phys. Fluids A*, Vol. 1, 1283 (1989).

[5] D. G. DRITSCHEL AND M. E. MCINTYRE, Does contour dynamics go singular?, *Phys. Fluids A*, Vol. 2, 748 (1990).

[6] D. G. DRITSCHEL AND N. J. ZABUSKY, A new, but flawed, numerical method for vortex patch evolution in two dimensions, *J. Comput. Phys.* Vol. 93, 481 (1991).

[7] T. F. BUTTKE, The fast adaptive vortex method, *J. Comput. Phys.* Vol. 93, 485 (1991).

[8] A. J. CHORIN AND J. E. MARSDEN, *A Mathematical Introduction to Fluid Mechanics*, (Springer-Verlag, New York, 1990).

[9] C. W. GEAR, *Numerical initial value problems in ordinary differential equations*, (Prentice-Hall, Englewood Cliffs, NJ 1971).

[10] H. LAMB, *Hydrodynamics*, (Dover, New York, 1945).

List of figure captions

Fig.1 A triangle in an appropriate coordinate system.

Fig.2 The configuration of the patches in Problem 1 at $T = 0.0$.

Fig.3 The configuration of the patches in Problem 1 at $T = 8.0$.

Fig.4 The configuration of the patches in Problem 1 at $T = 14.0$.

Fig.5 The configuration of the patches in Problem 2 at $T = 24.0$.

Fig.6 The details of Region A magnified by 35 times.

Fig.7 The curvature near Region A for different $\triangle t$.

Fig.8 The curvature near Region A for different $\triangle s$.

Fig. 1

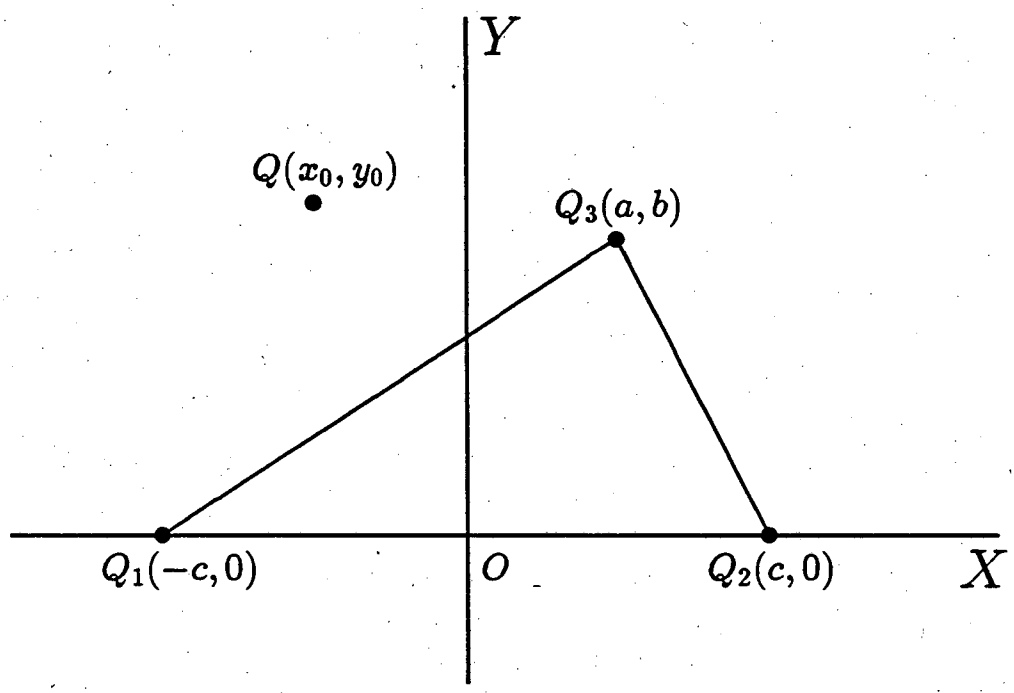

Fig. 2

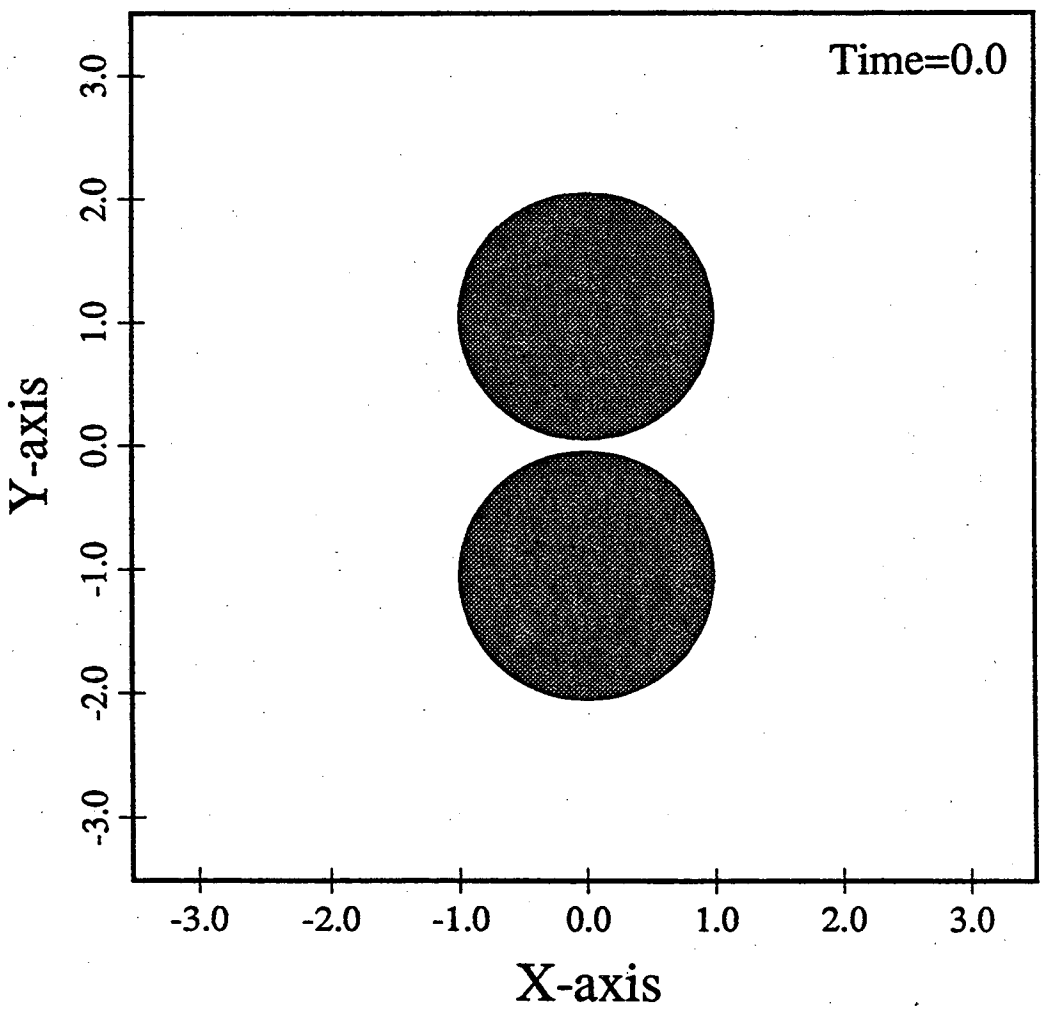

Fig. 3

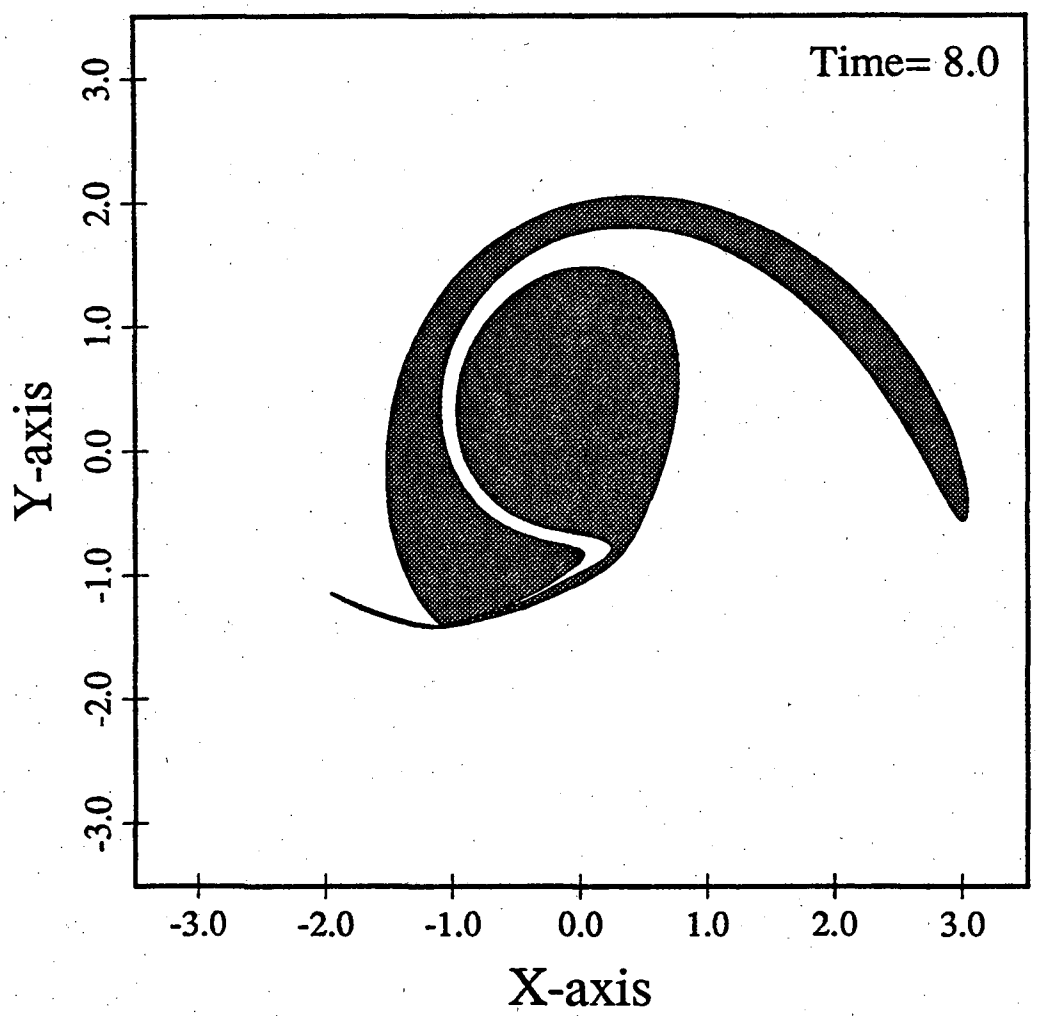

Fig. 4

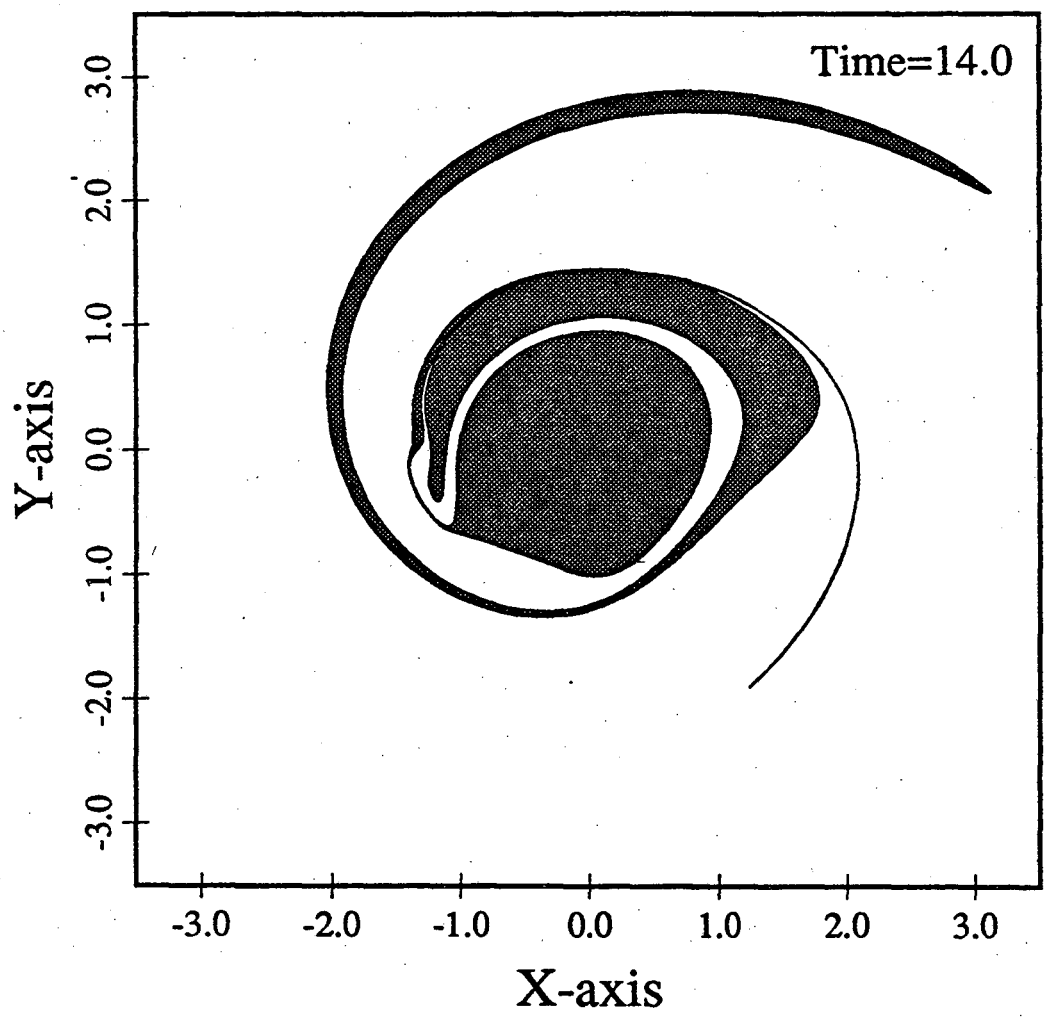

Fig. 5

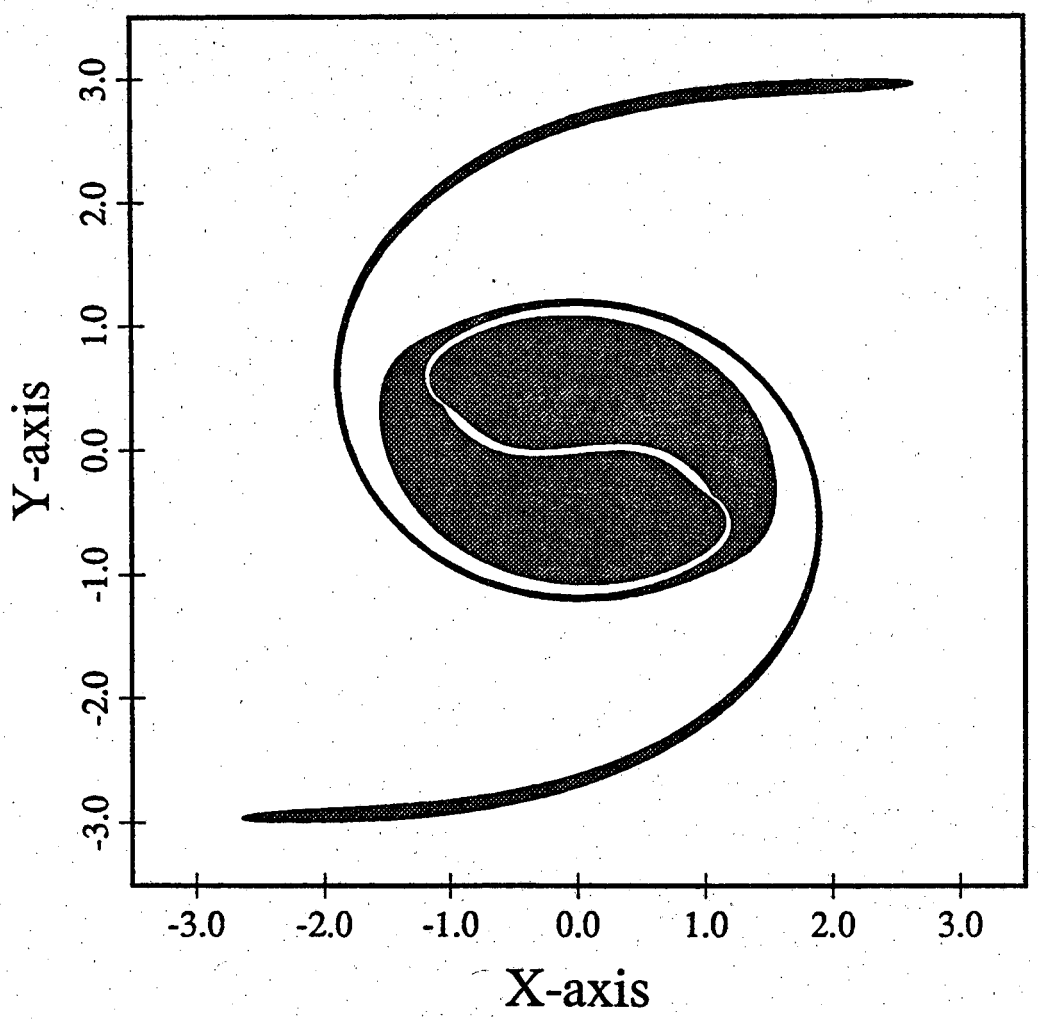

Fig. 6

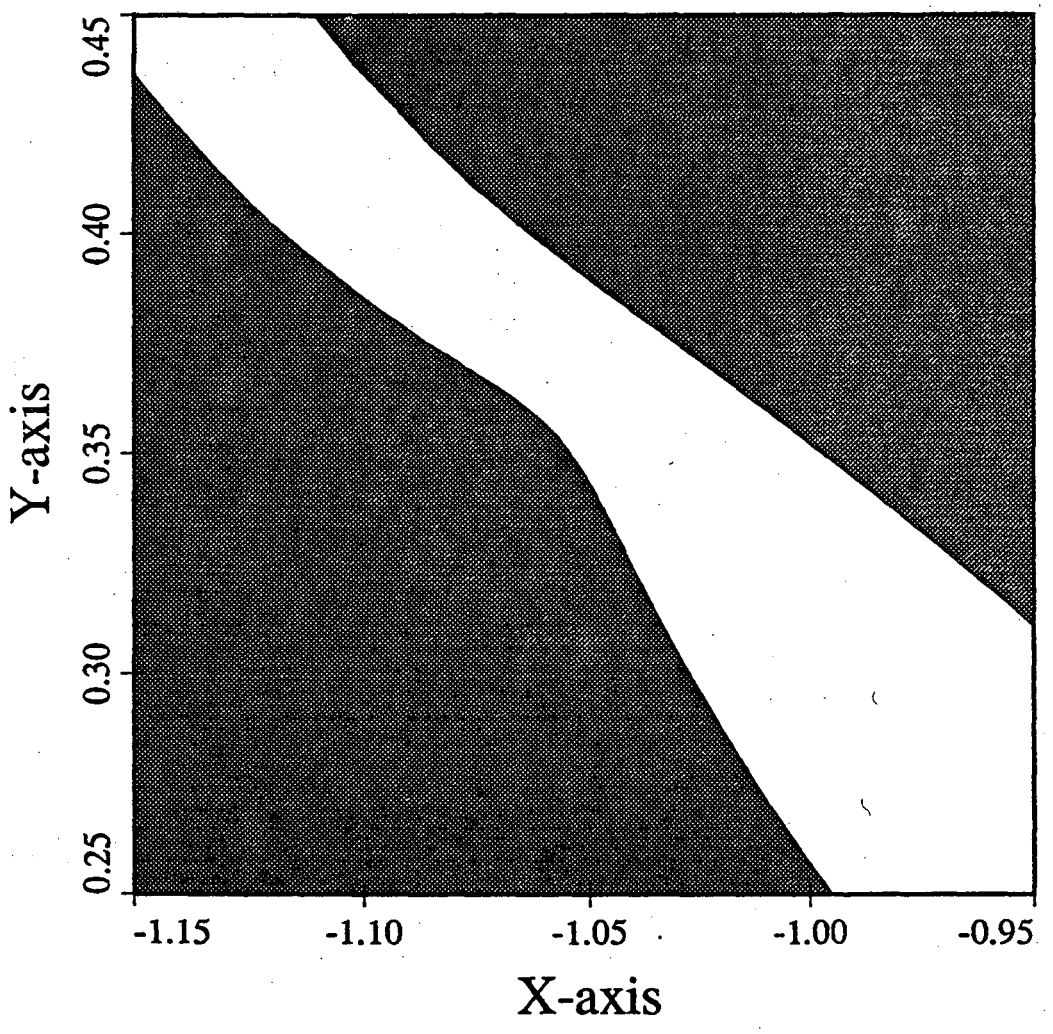

Fig. 7

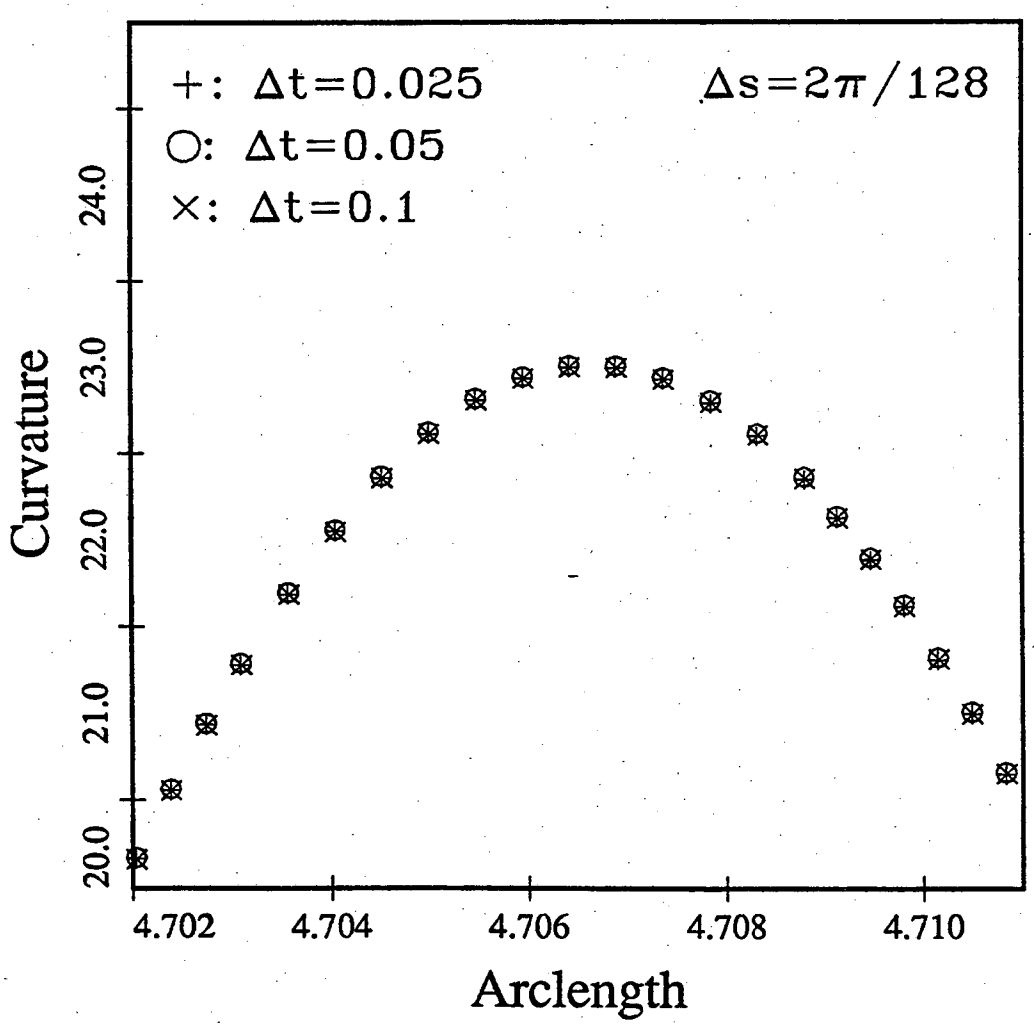
+: Δt=0.025
○: Δt=0.05
×: Δt=0.1
Δs=2π/128
Curvature
20.0
21.0
22.0
23.0
24.0
4.702
4.704
4.706
4.708
4.710
Arclength

Fig. 8

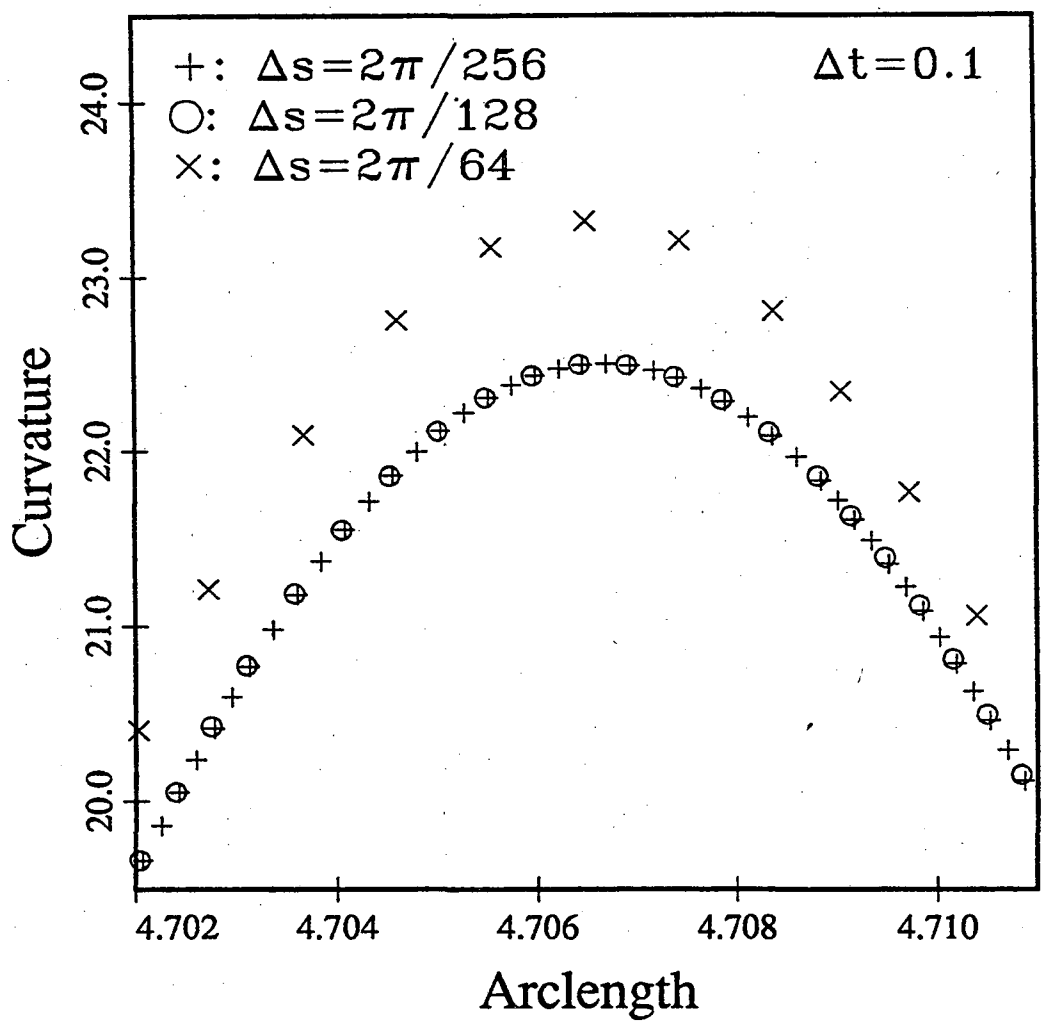
+: Δs=2π/256
○: Δs=2π/128
×: Δs=2π/64
Δt=0.1
Curvature
24.0
23.0
22.0
21.0
20.0
4.702
4.704
4.706
4.708
4.710
Arclength

LAWRENCE BERKELEY LABORATORY
UNIVERSITY OF CALIFORNIA
TECHNICAL INFORMATION DEPARTMENT
BERKELEY, CALIFORNIA 94720

ABH322
LBL Libraries